

Two-stream sausage and hollowing instabilities in high-intensity particle beams

Han S. Uhm

Department of Molecular Science and Technology, Ajou University, Suwon 442-749, Korea

Ronald C. Davidson and Igor Kaganovich

Plasma Physics Laboratory, Princeton University, Princeton, New Jersey 08543

(Received 26 March 2001; accepted 27 April 2001)

Axisymmetric two-stream instabilities in high-intensity particle beams are investigated analytically by making use of the Vlasov–Maxwell equations in the smooth-focusing approximation. The eigenfunctions for the axisymmetric radial modes are calculated self-consistently in order to determine the dispersion relation describing collective stability properties. Stability properties for the sausage and hollowing modes, characterized by radial mode numbers $n=1$ and $n=2$, respectively, are investigated, and the dispersion relations are obtained for the complex eigenfrequency ω in terms of the axial wavenumber k and other system parameters. The eigenfunctions obtained self-consistently for the sausage and hollowing modes indicate that the perturbations exist only inside the beam. Therefore, the location of the conducting wall does not have an effect on stability behavior. The growth rates of the sausage and hollowing modes are of the same order of magnitude as that of the hose (dipole-mode) instability. Therefore, it is concluded that the axisymmetric sausage and hollowing instabilities may also be deleterious to intense ion beam propagation when a background component of electrons is presented. © 2001 American Institute of Physics. [DOI: 10.1063/1.1403375]

I. INTRODUCTION

Charged particle beams are subject to various collective instabilities that can deteriorate the beam quality. For example, intense charged particle beams can develop a halo structure during propagation. This halo structure may be caused by collective excitations, such as axisymmetric hollowing instabilities. High energy ion accelerators and transport systems^{1–4} have a wide range of applications, including basic scientific research, spallation neutron sources, nuclear waste transmutation, and heavy ion fusion.^{5–7} However, background electrons are often present at the high beam currents and charge densities of practical interest in many ion beam applications. It has been recognized^{8–16} for many years that the relative streaming motion of the high-intensity beam particles through a background charge species can provide the free energy to drive the classical two-stream instability. For example, for electrons interacting with an intense proton beam, as in the Proton Storage Ring (PSR) experiment, or the Spallation Neutron Source (SNS), this instability is referred to as electron–proton ($e-p$) two-stream instability.^{11,12} Theoretical treatments of the two-stream instability can be based on either a kinetic model¹⁶ that makes use of the Vlasov–Maxwell equations to describe the self-consistent interaction of the ion and electron distribution functions with the applied field and the self-generated electric and magnetic fields, or on rigid-beam models^{9,17} that analyze the transverse motion of the center-of-mass of the ion and electron charge distributions. In the present analysis, we investigate two-stream instability properties for axisymmetric perturbations ($\partial/\partial\theta=0$) about an intense ion beam propagating through background electrons by making use of

the Vlasov–Maxwell equations. Therefore, the present work is complimentary to a previous study¹⁶ of the two-stream instability carried out for nonaxisymmetric perturbations ($\partial/\partial\theta\neq 0$).

The basic assumptions and theoretical model are summarized in Sec. II. The theoretical analysis is based on the linearized Vlasov–Maxwell equations assuming long-wavelength, low-frequency, axisymmetric perturbations with $\partial/\partial\theta=0$. The perturbation analysis is carried out for the specific choice of equilibrium distribution function in which all of the beam ions have the same value of transverse energy. The electrons are also assumed to have the same value of transverse energy. The eigenfunctions for axisymmetric radial modes are calculated self-consistently in order to obtain the dispersion relation for the complex eigenfrequency ω . The orbit integral for the perturbed distribution function is evaluated self-consistently by integrating over the unperturbed particle orbits, and the dispersion relation is obtained in matrix form [Eq. (26)] for radial mode numbers $n=1$ and $n=2$.

Stability properties of the *sausage mode*, characterized by the radial mode number $n=1$, are investigated in Sec. III. At moderate beam intensity, the dispersion relation for the sausage mode is approximated by a quadratic equation for the eigenfrequency ω , which has a qualitatively similar form to the dispersion relation for the dipole-mode instability (hose mode).¹⁶ The eigenfunction obtained self-consistently for the sausage mode indicates that the perturbations exist only inside the beam. Therefore, the location of the grounded conducting wall does not affect the stability behavior. Stability properties of the *hollowing instability*, characterized by

radial mode number $n=2$, are investigated in Sec. IV. The eigenfunction obtained self-consistently for the hollowing instability also indicates that the perturbations exist only inside the beam. The radial component of the perturbed electromagnetic force is proportional to the derivative of the effective perturbed potential with respect to the radial coordinate r , and displaces the beam particles towards the vicinity of the beam edge, thereby (nonlinearly) depleting the particle density on-axis ($r=0$). The full dispersion relation for the hollowing mode is obtained, and is approximated by a quadratic form at moderate beam intensity, which predicts instability for several ranges of axial wavenumber k . The growth rates of the sausage and hollowing modes are the same order-of-magnitude as those of the dipole-mode instability.¹⁶ In this regard, we emphasize that the axisymmetric sausage and hollowing instabilities may also be deleterious to intense ion beam propagation when a background component of electrons is present. Variations of the hose, sausage and hollowing instabilities^{18–21} are also known to affect the propagation of intense electron beams through background plasma.

II. BASIC ASSUMPTIONS AND THEORETICAL MODEL

The equilibrium configuration consists of an intense ion beam with radius r_b that propagates in the z direction with directed kinetic energy $(\gamma_b - 1)m_b c^2$ through a perfectly conducting cylinder with wall radius r_w . The ion beam propagates through background (stationary) electrons with characteristic directed axial momentum $\gamma_b m_b \beta_b c$ in the z direction, where $V_b = \beta_b c = \text{const}$ is the average axial velocity, and $\gamma_b = (1 - \beta_b^2)^{-1/2}$ is the relativistic mass factor. In order to simplify the analysis, it is assumed that the background column of electrons also has the radius r_b . In the context of the smooth-focusing approximation, the beam ions are radially confined by the applied transverse focusing force modeled by

$$F_{\text{foc}}^b = -\gamma_b m_b \omega_{\beta b}^2 \mathbf{x}_\perp, \quad (1)$$

where $\mathbf{x}_\perp = x\mathbf{e}_x + y\mathbf{e}_y$ is the transverse displacement from the beam axis, m_b is the ion rest mass, c is the speed of light *in vacuo*, and $\omega_{\beta b} = \text{const}$ is the effective betatron frequency for transverse ion motion in the applied focusing field. The equilibrium and stability analyses are carried out by using cylindrical polar coordinates (r, θ, z) , where the z axis is along the beam propagation direction, and r is the radial distance from the z axis. Both the ion beam and background electrons (in equilibrium), are assumed to be azimuthally symmetric ($\partial/\partial\theta=0$) and axially uniform ($\partial/\partial z=0$). As for the background electrons, to the extent that the beam ion density exceeds the background electron density, the space-charge force on an electron, $F_s^e = e\nabla\phi$, provides transverse confinement of the background electrons by the electrostatic space-charge potential $\phi(\mathbf{x}, t)$. However, for completeness, the present analysis also incorporates the effects of an *applied* transverse focusing force on the electrons modeled by $F_{\text{foc}}^e = -m_e \omega_{\beta e}^2 \mathbf{x}_\perp$, where m_e is the electron rest mass, and $\omega_{\beta e} = \text{const}$ is the effective betatron frequency for transverse electron motion in the applied focusing field. It is further assumed that the ion motion in the beam frame is nonrela-

tivistic, and that the transverse momentum components of a beam ion, p_x and p_y , and the characteristic spread in axial momentum, $\delta p_z = p_z - \gamma_b m_b \beta_b c$, are small in comparison with the directed axial momentum $\gamma_b m_b \beta_b c$.

Under the equilibrium assumption that the distribution function for the beam ions and background electrons are axisymmetric and spatially uniform in the axial direction, we recognize that the total transverse energies and axial momentum of the beam ions and background electrons are approximate constants of the motion in the equilibrium fields.¹⁶ For present purposes, the equilibrium distribution functions for the beam ions and the background electrons are taken to be¹⁶

$$F_b^0(H_{\perp b}, p_z) = \frac{n_b}{2\pi\gamma_b m_b} \delta(H_{\perp b} - T_{\perp b}) G_b(p_z),$$

$$F_e^0(H_{\perp e}, p_z) = \frac{n_e}{2\pi m_e} \delta(H_{\perp e} - T_{\perp e}) G_e(p_z). \quad (2)$$

Here, n_b and n_e are the on-axis ion and electron number densities, respectively, $T_{\perp b}$ and $T_{\perp e}$ are positive constants, and $H_{\perp b}$ and $H_{\perp e}$ are the single-particle Hamiltonians defined by

$$H_{\perp b} = \frac{1}{2\gamma_b m_b} p_\perp^2 + \frac{1}{2} \gamma_b m_b \omega_{\beta b}^2 r^2 + Z_b e [\Psi_0(r) - \Psi_{0m}],$$

$$H_{\perp e} = \frac{1}{2m_e} p_\perp^2 + \frac{1}{2} m_e \omega_{\beta e}^2 r^2 - e [\phi_0(r) - \phi_{0m}], \quad (3)$$

where $Z_b e$ is the ion charge, $-e$ is the electron charge, $\Psi_0(r)$ is defined by $\Psi_0(r) \equiv \phi_0(r) - \beta_b A_z(r)$, $\phi_0(r)$ is the equilibrium electrostatic potential, and $A_z(r)$ is the axial component of the equilibrium vector potential. In Eq. (3), $r = (x^2 + y^2)^{1/2}$ is the radial distance from the beam axis, and the axial momentum distributions are normalized according to

$$\int_{-\infty}^{\infty} G_b(p_z) dp_z = 1 = \int_{-\infty}^{\infty} G_e(p_z) dp_z. \quad (4)$$

The equilibrium self-field potentials $\Psi_0(r)$ and $\phi_0(r)$ occurring in Eq. (3) are calculated self-consistently from¹⁶

$$\frac{1}{r} \frac{\partial}{\partial r} r \frac{\partial}{\partial r} \Psi_0(r) = -4\pi e \left[\frac{Z_b}{\gamma_b} n_b^0(r) - n_e^0(r) \right],$$

$$\frac{1}{r} \frac{\partial}{\partial r} r \frac{\partial}{\partial r} \phi_0(r) = -4\pi e [Z_b n_b^0(r) - n_e^0(r)], \quad (5)$$

and the equilibrium ion and electron density profiles, $n_b^0(r)$ and $n_e^0(r)$, are defined by

$$n_b^0(r) = \int d^3p F_b^0(H_{\perp b}, p_z),$$

$$n_e^0(r) = \int d^3p F_e^0(H_{\perp e}, p_z). \quad (6)$$

The constants Ψ_{0m} and ϕ_{0m} in Eq. (3) are the on-axis ($r=0$) values of the self-field potentials, $\Psi_0(r)$ and $\phi_0(r)$, and Z_b is the ionization state of the ions, which is included here to extend the analysis to beam ions with a higher charge state than $Z_b=1$. Finally, in Eqs. (3) and (5), it has been

assumed that the equilibrium axial current, $J_z^0(r) = Z_b e n_b^0 V_{zb}^0$, is carried by the beam ions, with $V_{ze}^0 \approx \beta_e c = 0$.

In order to simplify subsequent analysis, we assume that the ion beam and background electrons have overlapping density profiles. Substituting Eq. (2) into Eq. (6), and making use of Eqs. (3), (4), and (5), we obtain the step-function density profiles

$$n_b^0(r) = \frac{n_e^0(r)}{Z_b f} = \begin{cases} n_b = \text{const}, & 0 \leq r < r_b \\ 0, & r_b < r \leq r_w \end{cases} \quad (7)$$

where $f = n_e / Z_b n_b = \text{const}$ is the fractional charge neutralization by the background electrons. In Eq. (7), the equilibrium beam radius r_b is defined by

$$r_b^2 = 2 \frac{T_{\perp b}}{\gamma_b m_b v_b^2} = 2 \frac{T_{\perp e}}{m_e v_e^2}, \quad (8)$$

where the (depressed) betatron frequencies, ν_b and ν_e in Eq. (8) for the beam ions and background electrons are defined by¹⁶

$$\begin{aligned} \nu_b^2 &= \omega_{\beta b}^2 - \frac{\omega_{pb}^2}{2} \left(\frac{1}{\gamma_b^2} - f \right), \\ \nu_e^2 &= \omega_{\beta e}^2 + \frac{\omega_{pe}^2}{2} \frac{\gamma_b m_b}{Z_b m_e} (1 - f). \end{aligned} \quad (9)$$

The constant $f = n_e / Z_b n_b$ in Eqs. (7) and (9) represents the fractional charge neutralization provided by the background electrons. The quantity ω_{pb}^2 occurring in Eq. (9) is the on-axis relativistic beam plasma frequency-squared defined by $\omega_{pb}^2 = 4 \pi n_b Z_b^2 e^2 / \gamma_b m_b$. As expected, the (depressed) betatron frequencies in Eq. (9) for the ions and electrons inside the beam are constants (independent of radial coordinate r) for the step-function density profiles in Eq. (7).

We now make use of linearized Vlasov–Maxwell equations¹⁶ to develop a theoretical model of the two-stream instability for perturbations about the equilibrium described by Eq. (2). In the subsequent analysis, we adopt a normal mode approach in which all perturbed quantities are assumed to vary with θ , z , and t according to

$$\delta \Gamma(r, \theta, z, t) = \Gamma_1(r) \exp[i(kz - \omega t)], \quad (10)$$

for axisymmetric perturbations with $\partial / \partial \theta = 0$. Here, ω and k are the complex eigenfrequency and axial wavenumber of the perturbation, with $\text{Im} \omega > 0$ corresponding to temporal growth. We also consider axial wavelengths that are long and frequencies that are low compared with quantities that characterize the beam radius, i.e.,

$$|kr_b| \ll 1, \quad |\omega r_b| \ll c. \quad (11)$$

Furthermore, the present stability analysis assumes electrostatic perturbations with sufficiently high frequency that $|\omega/k - \beta_b c| \gg \nu_{Tbz}$ and $|\omega/k| \gg \nu_{Tez}$, where $\nu_{Tbz} = (2T_{bz} / \gamma_b^3 m_b)^{1/2}$ and $\nu_{Tez} = (2T_{ez} / m_e)^{1/2}$ are the characteristic axial thermal speeds of the beam ions and the background electrons, respectively. Indeed, for present purposes, we assume $G_b(p_z) = \delta(p_z - \gamma_b m_b \beta_b c)$ and $G_e(p_z) = \delta(p_z)$, which correspond to beam ions and background electrons

that are cold in the axial direction. The perturbed potential amplitudes, $\Psi_1(r)$ and $\phi_1(r)$, for the beam ions and background electrons occurring in the linearized Vlasov equations are determined self-consistently in terms of the perturbed particle number densities. We obtain

$$\begin{aligned} \frac{\partial}{\partial r} \frac{1}{r} \frac{\partial}{\partial r} r \psi_1(r) &= -4 \pi e \left[\frac{Z_b}{\gamma_b^2} n_{b1}(r) - n_{e1}(r) \right], \\ \frac{\partial}{\partial r} \frac{1}{r} \frac{\partial}{\partial r} r \phi_1(r) &= -4 \pi e [Z_b n_{b1}(r) - n_{e1}(r)], \end{aligned} \quad (12)$$

where $\psi_1(r) = \phi_1(r) - \beta_b A_{z1}(r)$, and $n_{b1}(r)$ and $n_{e1}(r)$ are the perturbed number densities of the beam ions and background electrons, respectively. The perturbed densities can be obtained from the linearized Vlasov equations for δF_b and δF_e . For example, the perturbed ion beam density $n_{b1}(r)$ is calculated from

$$n_{b1}(r) = \int d^3 p \delta F_b. \quad (13)$$

In Eq. (13), δF_b is the perturbed ion beam distribution function calculated by the method of the characteristics¹ which can be expressed as¹⁶

$$\begin{aligned} \delta F_b(\mathbf{x}, \mathbf{p}, t) &= Z_b e G_b(p_z) \frac{\partial}{\partial H_{\perp b}} F_{b0}(H_{\perp b}) \int_{-\infty}^t dt' \frac{\mathbf{p}'_{\perp}}{\gamma_b m_b} \\ &\quad \cdot \nabla_{\perp} \delta \psi(\mathbf{x}', t'), \end{aligned} \quad (14)$$

where use has been made of Eq. (11). Here, $\mathbf{x}'(t')$ and $\mathbf{p}'(t')$ are the particle trajectories in the equilibrium field configuration that pass through the phase space point (\mathbf{x}, \mathbf{p}) at time $t' = t$.

We note from Eq. (14) that the time integral requires information on the particle orbits in the equilibrium fields. A determination of the particle orbit in the equilibrium fields, generated by the self-field potentials $\Psi_0(\mathbf{x})$ and $\phi_0(\mathbf{x})$ in Eq. (5), is difficult for general equilibrium profiles. Moreover, Eq. (14) contains an integral over the unperturbed orbits of the (yet unknown) eigenfunction $\delta \psi$, which makes Eq. (12) generally intractable analytically. This difficulty is fundamental, reflecting the fact that individual particle orbits span the beam cross section, communicating information about the perturbation from one value of r to another. However, the particle motion in the equilibrium field configuration generated by the step-function density profile in Eq. (7) can be determined exactly.¹⁰

It is convenient to introduce the effective perturbed potential amplitude $\psi_j(r)$ defined by

$$\psi_j(r) = \phi_1(r) - \beta_j A_{z1}(r) \quad (15)$$

for charge species j in a frame of reference moving with axial velocity $\beta_j c$. Here, $A_{z1}(r)$ is the axial component of the perturbed vector potential. Note that the axial velocity $\beta_j c$ of the beam ions and the background electrons are given by $\beta_j = \beta_b$ for the beam ions ($j = b$) and $\beta_j = 0$ for the background electrons ($j = e$). After carrying out some tedious but straightforward algebraic manipulation of Eqs. (2), (3), (13), (14), and (15), we obtain the coupled integro-differential equations²² for the eigenfunctions $\psi_s(r)$

$$\begin{aligned} & \frac{1}{r} \frac{d}{dr} r \frac{d}{dr} \psi_s(r) \\ &= \delta(r-r_b) \sum_j \frac{4\pi e_j^2 n_j}{\gamma_j m_j \nu_j^2 R_b} (1-\beta_s \beta_j) \\ & \quad \times [\psi_j(R_b) + \Omega_j I_j(R_b)] + \Theta(r_b-r) \\ & \quad \times \sum_j 8\pi \gamma_j m_j e_j^2 n_j \Omega_j (1-\beta_s \beta_j) \left(\frac{\partial I_j}{\partial p_\perp^2} \right)_{p_\perp^2=p_{0j}^2}. \end{aligned} \quad (16)$$

In Eq. (16), note that the contribution proportional to $\delta(r-r_b)$ corresponds to a surface perturbation localized at $r=r_b$ whereas the term proportional to $\Theta(r_b-r)$ corresponds to a body wave perturbation extending throughout the beam. The orbit integral I_j in Eq. (16) is defined by

$$I_j(r, p_\perp) = i \int_0^{2\pi} \frac{d\varphi}{2\pi} \int_{-\infty}^0 d\tau \psi_j(r') \exp(i\Omega_j \tau). \quad (17)$$

Here, $\tau=t'-t$ is the displaced time variable, the transverse kinetic energy of the particles occurring in Eq. (16) is defined by

$$\frac{p_{0j}^2}{2\gamma_j m_j} = \frac{1}{2} \gamma_j m_j \nu_j^2 (r_b^2 - r^2), \quad (18)$$

and the Doppler-shifted eigenfrequency Ω_j is defined by

$$\Omega_j = \begin{cases} \omega - k\beta_b c, & j=b, \\ \omega, & j=e. \end{cases} \quad (19)$$

The function $\Theta(x)$ on the right-hand side of Eq. (16) is the Heaviside function defined by $\Theta(x)=1$ for $x>0$ and $\Theta(x)=0$ for $x<0$. The subscript s in Eq. (16) represents the beam ions for $s=b$ and the background electrons for $s=e$, and therefore the charge e_j occurring in Eq. (16) is given by

$$e_j = \begin{cases} Ze, & j=b, \\ -e, & j=e. \end{cases} \quad (20)$$

The angle φ occurring in the orbit integral in Eq. (16) is the perpendicular momentum phase angle defined by $p_x = p_\perp \cos \varphi$ and $p_y = p_\perp \sin \varphi$. Note that the orbit integral in Eq. (17) must be carried out in order to solve the coupled eigenvalue equations (16). For the step-function density profiles in Eq. (7), the particle orbits are given by^{16,22}

$$\begin{aligned} x'(\tau) &= \frac{p_\perp}{\gamma_j m_j \nu_j} \cos \varphi \sin \nu_j \tau + r \cos \theta \cos \nu_j \tau, \\ y'(\tau) &= \frac{p_\perp}{\gamma_j m_j \nu_j} \sin \varphi \sin \nu_j \tau + r \sin \theta \cos \nu_j \tau, \end{aligned} \quad (21)$$

where ν_j is the (depressed) betatron frequency defined in Eq. (9), and $\tau=t'-t$ is the displaced time variable. The boundary condition of the particle orbit are $x(\tau=0)=x=r \cos \theta$ and $y(\tau=0)=y=r \sin \theta$. The beam ions and the background electrons execute the simple harmonic orbits described by Eq. (21) over the beam cross section.

The self-consistent eigenfunctions $\psi_b(r)$ and $\psi_e(r)$ for radial mode number n are given by²²

$$\psi_j(r) = \begin{cases} \sum_{\alpha=0}^n a_{j\alpha} \left(\frac{r}{r_b} \right)^{2\alpha}, & 0 < r < r_b, \\ \frac{\ln(r/r_w)}{\ln(r_b/r_w)} \sum_{\alpha=0}^n a_{j\alpha}, & r_b < r < r_w, \end{cases} \quad (22)$$

where r_w is the radius of the conducting cylinder, and $a_{j\alpha}$ are expansion coefficients. The orbit integral I_j in Eq. (17) can be calculated by substituting Eq. (22) into Eq. (17) and making use of the unperturbed orbit in Eq. (21). In order to evaluate the orbit integral I_j in Eq. (17), we use the relation

$$\begin{aligned} (r')^2 = (x')^2 + (y')^2 &= \frac{p_\perp^2}{\gamma_j^2 m_j^2 \nu_j^2} \sin^2 \nu_j \tau + r^2 \cos^2 \nu_j \tau \\ & \quad + \frac{r p_\perp}{\gamma_j m_j \nu_j} \cos(\varphi - \theta) \sin(2\nu_j \tau). \end{aligned} \quad (23)$$

We also introduce the time integrals, h_{cln}^j and h_{sln}^j , defined by

$$\begin{aligned} h_{cln}^j &= h[\cos^l(n\nu_j \tau)] \\ &= i\Omega_j \int_{-\infty}^0 d\tau \exp(-i\Omega_j \tau) \cos^l(n\nu_j \tau), \\ h_{sln}^j &= h[\sin^l(n\nu_j \tau)] \\ &= i\Omega_j \int_{-\infty}^0 d\tau \exp(-i\Omega_j \tau) \sin^l(n\nu_j \tau). \end{aligned} \quad (24)$$

A few examples of the time integrals defined in Eq. (24) have been calculated. They are

$$\begin{aligned} h_{c21}^j &= -\frac{\Omega_j^2 - 2\nu_j^2}{\Omega_j^2 - 4\nu_j^2}, & h_{s21}^j &= \frac{2\nu_j^2}{\Omega_j^2 - 4\nu_j^2}, \\ h_{s22}^j &= \frac{8\nu_j^2}{\Omega_j^2 - 16\nu_j^2}, \\ h_{c41}^j &= -\frac{\Omega_j^4 - 16\nu_j^2 \Omega_j^2 + 24\nu_j^4}{(\Omega_j^2 - 16\nu_j^2)(\Omega_j^2 - 4\nu_j^2)}, \\ h_{s41}^j &= -24 \frac{\nu_j^4}{(\Omega_j^2 - 16\nu_j^2)(\Omega_j^2 - 4\nu_j^2)}, \end{aligned} \quad (25)$$

which will be used to evaluate the orbit integral in Eq. (16).

We outline the solution to the coupled eigenvalue equations in Eq. (16) for the case of axisymmetric modes with radial mode numbers $n=1$ and $n=2$, which have the functional form in Eq. (22). We first substitute Eqs. (22) and (23) into Eq. (17), and evaluate the orbit integral I_j in terms of Ω_j and the coefficients $a_{j\alpha}$ by making use of Eqs. (24) and (25), thereby obtaining a closed form of the orbit integral. Next we substitute Eq. (21) into Eq. (15) and solve Eq. (15) inside the beam. Finally, we apply the appropriate boundary conditions at $r=r_b$, determined by multiplying Eq. (15) by r and integrating over the interval $r_b - \varepsilon < r < r_b + \varepsilon$, with $\varepsilon \rightarrow 0_+$. The result is a matrix dispersion equation of the form

$$\begin{pmatrix} \chi_{11} & 0 & \chi_{13} & \chi_{14} & \chi_{15} & \chi_{16} \\ 0 & \chi_{22} & \chi_{23} & \chi_{24} & \chi_{25} & \chi_{26} \\ 0 & 0 & \chi_{33} & \chi_{34} & \chi_{35} & \chi_{36} \\ 0 & 0 & \chi_{43} & \chi_{44} & \chi_{45} & \chi_{46} \\ 0 & 0 & 0 & 0 & \chi_{55} & \chi_{56} \\ 0 & 0 & 0 & 0 & \chi_{65} & \chi_{66} \end{pmatrix} \begin{pmatrix} a_{b0} \\ a_{e0} \\ a_{b1} \\ a_{e1} \\ a_{b2} \\ a_{e2} \end{pmatrix} = 0. \quad (26)$$

Here, the matrix elements in Eq. (26) are defined by

$$\begin{aligned} \chi_{11} &= [\ln(r_w/r_b)]^{-1}, & \chi_{13} &= \chi_{11} - \chi_{33}, & \chi_{14} &= -\chi_{34}, \\ \chi_{15} &= \chi_{11} - (1/2)\chi_{55} - \chi_{35}, & \chi_{16} &= -(1/2)\chi_{56} - \chi_{36}, \\ \chi_{22} &= \chi_{11}, & \chi_{23} &= -\chi_{43}, & \chi_{24} &= \chi_{11} - \chi_{44}, \\ \chi_{25} &= -(1/2)\chi_{65} - \chi_{45}, & \chi_{26} &= \chi_{11} - (1/2)\chi_{66} - \chi_{46}, \\ \chi_{33} &= (\omega_{pb}^2/\gamma_b^2\nu_b^2)h_{s21}^b - 2, & \chi_{34} &= (\eta f \omega_{pb}^2/\nu_e^2)h_{s21}^e, \\ \chi_{35} &= 2(\omega_{pb}^2/\gamma_b^2\nu_b^2)h_{s41}^b, & \chi_{36} &= 2(\eta f \omega_{pb}^2/\nu_e^2)h_{s41}^e, \\ \chi_{43} &= (\omega_{pb}^2/\nu_b^2)h_{s21}^b, & \chi_{44} &= (\eta f \omega_{pb}^2/\nu_e^2)h_{s21}^e - 2, \\ \chi_{45} &= -2(\omega_{pb}^2/\nu_b^2)h_{s41}^b, \\ \chi_{55} &= (\omega_{pb}^2/\gamma_b^2\nu_b^2)(h_{s22}^b - 2h_{s41}^b) - 8, \\ \chi_{46} &= 2(\eta f \omega_{pb}^2/\nu_e^2)h_{s41}^e, \\ \chi_{66} &= (\eta f \omega_{pb}^2/\nu_e^2)(h_{s22}^e - 2h_{s41}^e) - 8, \\ \chi_{56} &= -(\eta f \omega_{pb}^2/\nu_e^2)(h_{s22}^e - 2h_{s41}^e), \\ \chi_{65} &= -(\omega_{pb}^2/\nu_b^2)(h_{s22}^b - 2h_{s41}^b), \end{aligned} \quad (27)$$

where η is defined by $\eta = \gamma_b m_b / Z_b m_e$, and $f = n_e / Z_b n_b$ is the fractional charge neutralization.

Setting the determinant of the matrix χ in Eq. (26) equal to zero gives the dispersion relation

$$\chi_{11}\chi_{22}(\chi_{33}\chi_{44} - \chi_{34}\chi_{43})(\chi_{55}\chi_{66} - \chi_{56}\chi_{65}) = 0. \quad (28)$$

Therefore, the dispersion relation for the $n = 1$ radial mode is obtained from

$$\chi_{33}\chi_{44} - \chi_{34}\chi_{43} = 0, \quad (29)$$

and the expansion coefficients in Eq. (26) for the $n = 1$ mode satisfy $a_{j0} \neq 0$, $a_{j1} \neq 0$, and $a_{j2} = 0$, where the subscript j represents $j = b$ for the beam ions and $j = e$ for the background electrons. The dispersion relation for $n = 2$ radial mode is obtained from

$$\chi_{55}\chi_{66} - \chi_{56}\chi_{65} = 0, \quad (30)$$

and the expansion coefficients $a_{j\alpha}$ in Eq. (26) for $n = 2$ mode are all nonzero. Stability properties for axisymmetric perturbations with radial mode numbers $n = 1$ and 2 are investigated in subsequent sections. It is also shown in subsequent sections that $\sum_{\alpha=0} a_{j\alpha} = 0$, which corresponds to $\psi_j(r = r_b) = 0$ at the beam surface and $\psi_j(r) = 0$ in vacuum region ($r_b < r \leq r_w$).

III. SAUSAGE-MODE STABILITY PROPERTIES FOR RADIAL MODE NUMBER $n = 1$

Axisymmetric perturbations with radial mode number $n = 1$ are characterized by the so-called sausage instability.²² The dispersion relation for the $n = 1$ mode is obtained from Eq. (29) by substituting Eqs. (25) and (27) into Eq. (29). Carrying out some straightforward algebraic manipulation, the dispersion relation for the $n = 1$ mode can be expressed as

$$[(\omega - k\beta_b c)^2 - \omega_b^2](\omega^2 - \omega_e^2) = \omega_f^4, \quad (31)$$

where ω_b and ω_e are defined by

$$\omega_b^2 = 4\omega_{\beta b}^2 - \omega_{pb}^2 \left(\frac{1}{\gamma_b^2} - 2f \right), \quad (32)$$

$$\omega_e^2 = (2 - f)\eta\omega_{pb}^2, \quad (33)$$

and the coupling term ω_f^4 is defined by

$$\omega_f^4 = \eta f \omega_{pb}^4. \quad (34)$$

In obtaining Eqs. (32) and (33), we have also made use of Eq. (9), assuming that there is no externally applied focusing force on the electrons ($\omega_{\beta e}^2 = 0$).

The dispersion relation in Eq. (31) is similar in general form to previous results^{15,16} obtained for the dipole-mode instability. In the absence of background electrons ($f = 0$), it follows from Eq. (34) that $\omega_f = 0$, and the dispersion relation in Eq. (31) gives purely oscillatory beam-mode sideband oscillations with frequency $\omega - k\beta_b c = \pm \omega_b$. For $f \neq 0$, however, it follows that $\omega_f \neq 0$, and the right-hand side of Eq. (31) causes an unstable coupling of the electron oscillations, $\omega = \pm \omega_e$, and the ion oscillations, $\omega - k\beta_b c = \pm \omega_b$, at least for a certain range of the axial wavenumber k . Specifically, for the positive-frequency electron branch in Eq. (31) with $\omega \approx +\omega_e$, it can be shown that the dispersion relation in Eq. (31) supports one unstable solution with $\text{Im } \omega > 0$ for oscillation frequency and wavenumber (ω, k) in the vicinity of (ω_0, k_0) defined by $\omega_0 = \omega_e$ and $k_0\beta_b c = \omega_e + \omega_b$. Indeed, the positive-frequency electron branch ($\omega \approx +\omega_e$) couples unstably with the downshifted ion branch ($\omega - k\beta_b c \approx -\omega_b$). Substituting $\omega = \omega_0 + \delta\omega$, and $k = k_0 + \delta k$ into Eq. (31) gives

$$(2\omega_b - \delta\omega + \beta_b c \delta k)(\delta\omega - \beta_b c \delta k)(2\omega_0 + \delta\omega)\delta\omega = -\omega_f^4, \quad (35)$$

which is fully equivalent to Eq. (31).

Note that the parameter $\eta = \gamma_b m_b / Z_b m_e$ occurring in Eqs. (33)–(35) is much larger than unity for protons and more massive ions. In parameter regimes of practical interest, ω_e in Eq. (33) is much larger than ω_b and ω_f in Eqs. (32) and (34), and therefore $|\delta\omega| \ll 2\omega_e$. If further, $|\delta\omega|, |\beta_b c \delta k| \ll 2\omega_b$, then Eq. (35) can be approximated by the simple quadratic form

$$\delta\omega(\delta\omega - \beta_b c \delta k) = -\Gamma_0^2 \equiv -\frac{\omega_f^4}{4\omega_e\omega_b}, \quad (36)$$

which has a maximum growth rate $(\text{Im } \omega)_{\text{max}} = \Gamma_0$ when $\delta k = 0$. It is obvious from Eqs. (34) and (36) that the maximum

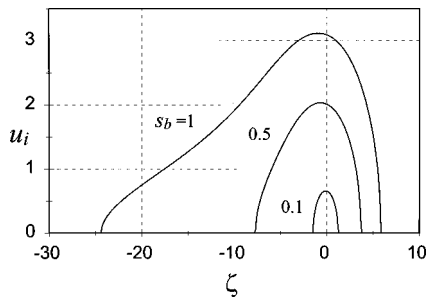


FIG. 1. Plots of the normalized growth rate $u_i = (\text{Im } \omega)/\omega_{\beta b}$ versus the shifted axial wavenumber $\zeta = (k - k_0)\beta_b c/\omega_{\beta b}$ obtained numerically from Eq. (31) for several values of normalized beam intensity $s_b = \omega_{pb}^2/2\gamma_b^2\omega_{\beta b}^2$ ranging from 0.1 to 1.0. Here, $k_0\beta_b c = \omega_e + \omega_b$. Other system parameters correspond to $Z_b = 1$, mass number $A = m_b/m_p = 137$, $(\gamma_b - 1)m_b c^2 = 2.5$ GeV, $f = 0.1$, and $\omega_{\beta e} = 0$.

growth rate Γ_0 in Eq. (36) increases as the fractional charge neutralization increases. We also note from Eq. (36) that the unstable range of the axial wavenumber k is given by $-2\Gamma_0 < \beta_b c \delta k < 2\Gamma_0$.

The quadratic approximation to the dispersion relation given in Eq. (36) is valid for moderate beam intensities satisfying $s_b = \omega_{pb}^2/2\gamma_b^2\omega_{\beta b}^2 \lesssim 0.2$. This is the case of interest for proton linacs and storage rings. For heavy ion fusion applications,⁵⁻⁷ however, the beam emittance is very low and the normalized beam intensity is such that s_b can approach unity in the absence of background electrons ($f = 0$). At such high beam intensities, it follows that it is necessary to solve the full quartic dispersion relation (31) for the complex oscillation frequency ω . Typical results obtained from Eq. (31) are illustrated in Fig. 1, where the normalized growth rate $u_i = (\text{Im } \omega)/\omega_{\beta b}$ is plotted versus the shifted axial wavenumber $\zeta = (k - k_0)\beta_b c/\omega_{\beta b}$ for several values of s_b ranging from 0.1 to 1.0. Here, $k_0\beta_b c = \omega_e + \omega_b$. Other system parameters in Fig. 1 correspond to $Z_b = 1$, mass number $A = m_b/m_p = 137$ (cesium ions), $(\gamma_b - 1)m_b c^2 = 2.5$ GeV, $f = 0.1$, and $\omega_{\beta e} = 0$. At very high beam intensity with $s_b = 1$, say, it is evident from Fig. 1 that the normalized growth rate u_i has a large bandwidth and becomes significantly skewed about $k = k_0$. It is also striking from Fig. 1 that the instability growth rate can be large for the very high beam intensities ($s_b \rightarrow 1$) of interest for heavy ion fusion. The normalized real frequency $\text{Re } \omega$ can also be obtained numerically from Eq. (31). Profiles of the normalized real frequency of the sausage instability are qualitatively similar to those of the dipole mode.¹⁶

The maximum growth rate $(\text{Im } \omega)_{\text{max}}$ obtained from the quadratic approximation in Eq. (36) occurs at $\zeta = 0$. The maximum growth rate for high beam intensity obtained from full dispersion relation in Eq. (31) still occurs in the vicinity of $k = k_0$, although it is skewed about $k = k_0$. Shown in Fig. 2 are plots of the normalized growth rate $u_i = (\text{Im } \omega)/\omega_{\beta b}$ versus the intensity parameter s_b obtained from Eqs. (31) and (36) for $k = k_0$ and parameters otherwise identical to Fig. 1. For sufficiently small values of s_b , the numerical results obtained from Eq. (31) are in excellent agreement with the approximate quadratic dispersion relation in Eq. (36). On the other hand, at very high beam intensity with $s_b \rightarrow 1$, the

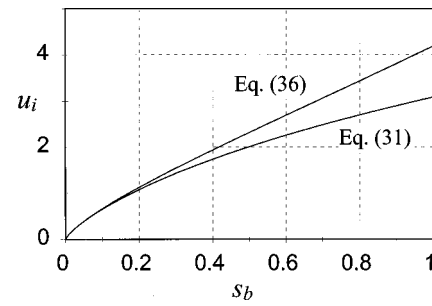


FIG. 2. Plots of the normalized growth rate $u_i = (\text{Im } \omega)/\omega_{\beta b}$ versus normalized beam intensity $s_b = \omega_{pb}^2/2\gamma_b^2\omega_{\beta b}^2$ obtained from Eqs. (31) and (36) for $k = k_0$ and parameters otherwise identical to Fig. 1.

maximum growth rate obtained from the approximate dispersion relation in Eq. (36) is an overestimate by about 35% relative to the maximum growth rate obtained from the full dispersion relation in Eq. (31). In summary, the growth-rate properties of the sausage instability characterized by axisymmetric perturbations with radial mode $n = 1$ are qualitatively similar to those of the dipole-mode instability described previously.¹⁶ The real oscillation frequency for the sausage mode, however, is found to be larger than that of the dipole-mode instability.

It is important to note that the dispersion relation in Eq. (31) is independent of the radial location of the conducting wall. Moreover, the eigenfunctions for the $n = 1$ radial mode are given by

$$\begin{aligned}\psi_b(r) &= a_{b0} + a_{b1}(r/r_b)^2, \\ \psi_e(r) &= a_{e0} + a_{e1}(r/r_b)^2,\end{aligned}\quad (37)$$

inside the beam ($0 \leq r < r_b$). From Eq. (26), we obtain

$$\begin{aligned}\chi_{11}a_{b0} + \chi_{13}a_{b1} + \chi_{14}a_{e1} &= 0, & \chi_{33}a_{b1} + \chi_{34}a_{e1} &= 0, \\ \chi_{22}a_{e0} + \chi_{23}a_{b1} + \chi_{24}a_{e1} &= 0, & \chi_{43}a_{b1} + \chi_{44}a_{e1} &= 0,\end{aligned}\quad (38)$$

where the matrix element χ_{22} is equal to χ_{11} . The coefficients a_{b0} , a_{e0} , a_{b1} , and a_{e1} are determined from Eq. (38), by making use of the dispersion relation in Eq. (29). Making use of Eqs. (27) and (38), it is straightforward to show $a_{b0} = -a_{b1}$ and $a_{e0} = -a_{e1}$. Therefore, from Eqs. (22) and (37), it follows $\psi_j(r) = 0$ for $(r_b < r \leq r_w)$. This means that the perturbed electromagnetic fields of the axisymmetric sausage mode are zero in vacuum region outside the beam. Sausage-mode perturbations do not sense the presence of the conducting wall. Thus, the dispersion relation in Eq. (31) does not depend on the location of the conducting wall.

IV. HOLLOWING-MODE STABILITY PROPERTIES FOR RADIAL MODE NUMBER $n = 2$

It is instructive to determine the eigenfunctions in Eq. (28) for the $n = 2$ radial mode. The first pair of equations relating the coefficients of the $n = 2$ eigenfunctions are given by

$$\begin{aligned}\chi_{11}a_{b0} + \chi_{13}a_{b1} + \chi_{14}a_{e1} + \chi_{15}a_{b2} + \chi_{16}a_{e2} &= 0, \\ \chi_{11}a_{e0} + \chi_{23}a_{b1} + \chi_{24}a_{e1} + \chi_{25}a_{b2} + \chi_{26}a_{e2} &= 0,\end{aligned}\quad (39)$$

which follow from the matrix equation (26). Equation (39) can be simplified to give

$$a_{b0} + a_{b1} + a_{b2} = 0, \quad a_{e0} + a_{e1} + a_{e2} = 0, \quad (40)$$

where use has been made of the relationship between the matrix elements in Eq. (27). The second pair of equations relating the coefficients of the $n = 2$ eigenfunctions are also obtained from Eq. (26) and are given by

$$\begin{aligned} \chi_{33}a_{b1} + \chi_{34}a_{e1} + \chi_{35}a_{b2} + \chi_{36}a_{e2} &= 0, \\ \chi_{43}a_{b1} + \chi_{44}a_{e1} + \chi_{45}a_{b2} + \chi_{46}a_{e2} &= 0. \end{aligned} \quad (41)$$

From the identity $4 \sin^4 \alpha = 4 \sin^2 \alpha - (\sin 2\alpha)^2$, we obtain the relation

$$h_{s21}^j = h_{s41}^j + (1/4)h_{s22}^j = (1/4)(h_{s22}^j - 2h_{s41}^j) + (3/2)h_{s41}^j, \quad (42)$$

from Eq. (24). Therefore, by making use of the matrix elements in Eq. (27), we obtain

$$\begin{aligned} \chi_{33} &= \frac{1}{4}\chi_{55} + \frac{3}{4}\chi_{35}, & \chi_{34} &= \frac{1}{4}\chi_{56} + \frac{3}{4}\chi_{36}, \\ \chi_{43} &= \frac{1}{4}\chi_{65} + \frac{3}{4}\chi_{45}, & \chi_{44} &= \frac{1}{4}\chi_{66} + \frac{3}{4}\chi_{46}. \end{aligned} \quad (43)$$

Substitution of Eq. (43) into Eq. (41) then gives

$$\begin{aligned} \chi_{35}[(3/4)a_{b1} + a_{b2}] + \chi_{36}[(3/4)a_{e1} + a_{e2}] \\ + (1/4)(\chi_{55}a_{b1} + \chi_{56}a_{e1}) &= 0, \\ \chi_{45}[(3/4)a_{b1} + a_{b2}] + \chi_{46}[(3/4)a_{e1} + a_{e2}] \\ + (1/4)(\chi_{65}a_{b1} + \chi_{66}a_{e1}) &= 0. \end{aligned} \quad (44)$$

The final pair of equations relating the coefficients of the $n = 2$ eigenfunctions are given by

$$\begin{aligned} \chi_{55}a_{b2} + \chi_{56}a_{e2} &= 0, \\ \chi_{65}a_{b2} + \chi_{66}a_{e2} &= 0, \end{aligned} \quad (45)$$

which follow from Eq. (26). The axial component $A_{zj}(r)$ of the perturbed vector potential has the same radial profile as the perturbed electrostatic potential $\phi_1(r)$ for the electrostatic and magnetostatic perturbations characterized by long-wavelength ($|kr_b| \ll 1$), low-frequency ($|\omega r_b| \ll c$) perturbations. Therefore, it follows that $a_{b1}/a_{b2} = a_{e1}/a_{e2}$. Equation (44) can be simplified to give

$$\begin{aligned} \chi_{35}[(3/4)a_{b1} + a_{b2}] + \chi_{36}[(3/4)a_{e1} + a_{e2}] &= 0, \\ \chi_{45}[(3/4)a_{b1} + a_{b2}] + \chi_{46}[(3/4)a_{e1} + a_{e2}] &= 0, \end{aligned} \quad (46)$$

by making use of Eq. (45).

The dispersion relation for the $n = 2$ radial mode is obtained from Eq. (45) and is given by Eq. (30). We also note that $\chi_{35}\chi_{46} - \chi_{36}\chi_{45} \neq 0$ when Eq. (30) is satisfied. Therefore, the coefficients in Eq. (46) are related by

$$(3/4)a_{b1} + a_{b2} = 0, \quad (3/4)a_{e1} + a_{e2} = 0. \quad (47)$$

Finally, making use of Eqs. (40) and (47), the eigenfunctions in Eq. (22) for the $n = 2$ radial mode are given by

$$\psi_j(r) = \begin{cases} \alpha_{j0} \left[1 - 4 \left(\frac{r}{r_b} \right)^2 + 3 \left(\frac{r}{r_b} \right)^4 \right], & 0 \leq r < r_b, \\ 0, & r_b < r \leq r_w, \end{cases} \quad (48)$$

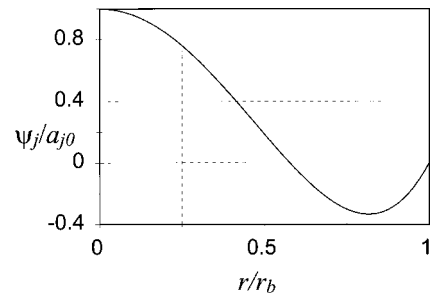


FIG. 3. Plot of the eigenfunction in Eq. (48) in terms of the normalized radial coordinate r/r_b .

which clearly indicates that the perturbed fields outside the beam vanish. Similar to the sausage mode, the stability properties of axisymmetric perturbations with radial mode number $n = 2$ do not depend on the location of the conducting wall.

Figure 3 shows a normalized plot of the eigenfunction in Eq. (48) versus the radial coordinate r/r_b . Note that the normalized eigenfunction $\psi_j(r)/a_{j0}$ has its maximum and minimum values at $r/r_b = 0$ and $r/r_b = 0.815$, respectively. The radial component of the perturbed electromagnetic force, which is proportional to the derivative of $d\psi(r)/dr$, changes sign at $r/r_b = 0.815$. Therefore, with an appropriate phase, the perturbed force, produced by the axisymmetric perturbations for the $n = 2$ radial mode, may push the inner beam particles toward the location $r/r_b = 0.815$, depleting the particle density near the beam axis. The term *hollowing instability* originates from this physical mechanism. On the other hand, the beam particles may also accumulate near the beam axis if the phase of the force is shifted by π radians.

Axisymmetric perturbations with radial mode number $n = 2$ are characterized by the so-called hollowing instability. The dispersion relation for the $n = 2$ mode is obtained from Eq. (30) by substituting Eqs. (25) and (27) into Eq. (30). Carrying out some straightforward algebraic manipulation, the dispersion relation for the $n = 2$ mode is given by

$$\begin{aligned} \left[(\Omega_b^2 - 16\nu_b^2)(\Omega_b^2 - 4\nu_b^2) - \frac{\omega_{pb}^2}{\gamma_b^2}(\Omega_b^2 + 2\nu_b^2) \right] \\ \times [(\omega^2 - 16\nu_e^2)(\omega^2 - 4\nu_e^2) - \eta f \omega_{pe}^2(\omega^2 + 2\nu_e^2)] \\ = f \eta \omega_{pb}^4 (\Omega_b^2 + 2\nu_b^2)(\omega^2 + 2\nu_e^2), \end{aligned} \quad (49)$$

where the Doppler-shifted frequency Ω_b is defined by $\Omega_b = \omega - k\beta_b c$ in Eq. (19), and the (depressed) betatron frequencies, ν_b and ν_e , are defined in Eq. (9). It is convenient to introduce the oscillation frequencies, $\omega_{b\pm}$ and $\omega_{e\pm}$, defined by

$$\omega_{b\pm}^2 = 10\nu_b^2 + \frac{\omega_{pb}^2}{2\gamma_b^2} \pm \sqrt{\left(10\nu_b^2 + \frac{\omega_{pb}^2}{2\gamma_b^2} \right)^2 - 2\nu_b^2 \left(32\nu_b^2 - \frac{\omega_{pb}^2}{\gamma_b^2} \right)} \quad (50)$$

for the beam ions, and

$$\omega_{e\pm}^2 = 10\nu_e^2 + \eta f \frac{\omega_{pb}^2}{2} \pm \sqrt{\left(10\nu_e^2 + \frac{\eta f}{2} \omega_{pb}^2\right)^2 - 2\nu_e^2(32\nu_e^2 - \eta f \omega_{pb}^2)} \quad (51)$$

for the background electrons. The dispersion relation in Eq. (49) for the axisymmetric $n=2$ mode can then be expressed in the equivalent form

$$\begin{aligned} & [(\omega - k\beta_b c)^2 - \omega_{b+}^2][(\omega - k\beta_b c)^2 - \omega_{b-}^2] \\ & \times (\omega^2 - \omega_{e-}^2)(\omega^2 - \omega_{e+}^2) \\ & = f\eta\omega_{pb}^4 [(\omega - k\beta_b c)^2 + 2\nu_b^2](\omega^2 + 2\nu_e^2), \end{aligned} \quad (52)$$

where the oscillation frequencies $\omega_{e\pm}$ and $\omega_{b\pm}$ satisfy the conditions $\omega_{b+} > \omega_{b-}$ and $\omega_{e+} > \omega_{e-}$.

In the absence of background electrons ($f=0$), Eq. (52) simplifies to give

$$[(\omega - k\beta_b c)^2 - \omega_{b+}^2][(\omega - k\beta_b c)^2 - \omega_{b-}^2] = 0, \quad (53)$$

which is identical to the dispersion relation obtained previously.^{1,22,23} Even for the limiting case where $f=0$, the quantity ω_{b-}^2 occurring in Eq. (50) can assume a negative value within a very limited range of beam parameters satisfying

$$\frac{16}{17} < \frac{\omega_{pb}^2}{2\gamma_b^2\omega_{\beta b}^2} < 1, \quad (54)$$

which has been obtained by making use of Eq. (9). Therefore, instability follows from Eq. (53) for an intense ion beam satisfying Eq. (54), which is very close to the space-charge-dominated limit where $s_b = \omega_{pb}^2/2\gamma_b^2\omega_{\beta b}^2 \rightarrow 1$. This well-known instability^{1,22-24} is associated with the inverted population in phase space of the Kapchinskij-Vladimirskij beam equilibrium²⁵ in Eq. (2), and has been investigated in numerical simulation studies²⁶⁻²⁸ of one-component beam propagation. The reader is urged to review Refs. 1 and 22-28 for further detailed information on the stability properties of high-intensity one-component particle beams.

We now consider the dispersion relation in Eq. (52) including the effects of a background electron component ($f = n_e/Z_in_b \neq 0$). Some straightforward algebra shows that $\omega_{b-}^2 > 0$, except for the narrow range of system parameters satisfying

$$1 - \frac{\omega_{pb}^2}{32\gamma_b^2\omega_{\beta b}^2} < \frac{\omega_{pb}^2}{2\omega_{\beta b}^2} \left(\frac{1}{\gamma_b^2} - f \right) < 1. \quad (55)$$

The right-most inequality in Eq. (55) is simply the condition $\nu_b^2 > 0$ [see Eq. (9)], required for existence of the equilibrium. Note that Eq. (55) reduces to Eq. (54) for $f=0$. In the subsequent analysis of the dispersion relation (52) for radial mode number $n=2$, we consider values of normalized beam intensity $s_b = \omega_{pb}^2/2\gamma_b^2\omega_{\beta b}^2$ and fractional charge neutralization f outside the interval in Eq. (55), in which case $\omega_{b-}^2 > 0$.

In the absence of background electrons ($f=0$), the dispersion relation in Eq. (52) gives purely oscillatory beam-

mode solutions with frequencies $\omega - k\beta_b c = \pm \omega_{b\pm}$. For $f \neq 0$, it follows that the right-hand side of Eq. (52) causes an unstable coupling of the electron oscillations, $\omega = \pm \omega_{e\pm}$, and the ion oscillations, $\omega - k\beta_b c = \pm \omega_{b\pm}$, at least for certain ranges of the axial wavenumber k . Specifically, for the positive-frequency electron branch in Eq. (52) with $\omega \approx +\omega_{e-}$, it is found that the dispersion relation in Eq. (52) supports one unstable solution for oscillation frequency and wavenumber (ω, k) in the vicinity of (ω_0, k_0) defined by $\omega_0 = \omega_{e-}$ and $k_0\beta_b c = \omega_{e-} - \omega_{b+}$, and another unstable solution in the vicinity of (ω_0, k_0) defined by $\omega_0 = \omega_{e-}$ and $k_0\beta_b c = \omega_{e-} + \omega_{b-}$. In other words, the positive-frequency electron branch ($\omega \approx +\omega_{e-}$) couples unstably with the upshifted ion branch ($\omega - k\beta_b c \approx \omega_{b+}$) corresponding to the axial wavenumber $k_0\beta_b c = \omega_{e-} - \omega_{b+}$, and also couples unstably with the downshifted ion branch ($\omega - k\beta_b c \approx -\omega_{b-}$) corresponding to the axial wavenumber $k_0\beta_b c = \omega_{e-} + \omega_{b-}$. For protons or more massive ions, note that the parameter $\eta = \gamma_b m_b / Z_b m_e$ is much larger than unity. In the parameter regimes of practical interest, the frequencies $\omega_{e\pm}$ in Eq. (52) are typically much larger than $\omega_{b\pm}$ and ω_{pb} , and therefore $|\delta\omega = \omega - \omega_{e\pm}| \ll 2\omega_{e\pm}$.

Equation (52) is an eighth-order polynomial dispersion relation which can be solved numerically for the complex oscillation frequency ω over a wide range of normalized beam intensity $s_b = \omega_{pb}^2/2\gamma_b^2\omega_{\beta b}^2$ and fractional charge neutralization $f = n_e/Z_in_b$. For our purposes here, to illustrate the essential features of the two-stream instability for the $n=2$ mode, we first consider Eq. (52) for moderate beam intensities with $s_b \leq 0.2$, say, a regime of considerable practical interest for high-intensity proton linacs and storage rings. In this case, $|\delta\omega|, |\beta_b c \delta k| \ll 2\omega_{b\pm}$ are good approximation, the dispersion relation in Eq. (52) for the positive-frequency electron branch with $\omega \approx +\omega_{e-}$ can be approximated by the quadratic form

$$\begin{aligned} & \delta\omega(\delta\omega - \beta_b c \delta k) \\ & = -\Gamma_1^2 = -f \frac{\eta}{4} \frac{\omega_{pb}^4}{\omega_{e-} - \omega_{b+}} \frac{(\omega_{b+}^2 + 2\nu_b^2)(\omega_{e-}^2 + 2\nu_e^2)}{(\omega_{b+}^2 - \omega_{b-}^2)(\omega_{e+}^2 - \omega_{e-}^2)}, \end{aligned} \quad (56)$$

in the vicinity of the axial wavenumber $k_0\beta_b c = \omega_{e-} - \omega_{b+}$, and by the quadratic form

$$\begin{aligned} & \delta\omega(\delta\omega - \beta_b c \delta k) \\ & = -\Gamma_2^2 = -f \frac{\eta}{4} \frac{\omega_{pb}^4}{\omega_{e-} - \omega_{b-}} \frac{(\omega_{b-}^2 + 2\nu_b^2)(\omega_{e-}^2 + 2\nu_e^2)}{(\omega_{b+}^2 - \omega_{b-}^2)(\omega_{e+}^2 - \omega_{e-}^2)}, \end{aligned} \quad (57)$$

in the vicinity of the axial wavenumber $k_0\beta_b c = \omega_{e-} + \omega_{b-}$. Here, $\delta\omega = \omega - \omega_{e-}$ and $\delta k = k - k_0$.

For the positive-frequency electron branch in Eq. (52) with $\omega \approx +\omega_{e+}$, it is also readily shown that the dispersion relation in Eq. (52) supports one unstable solution for oscillation frequency and wavenumber (ω, k) in the vicinity of (ω_0, k_0) defined by $\omega_0 = \omega_{e+}$ and $k_0\beta_b c = \omega_{e+} - \omega_{b-}$, corresponding to the upshifted ion branch with $\omega - k\beta_b c \approx +\omega_{b-}$, and another unstable solution in the vicinity of

(ω_0, k_0) defined by $\omega_0 = \omega_{e+}$ and $k_0\beta_b c = \omega_{e+} + \omega_{b+}$, corresponding to the downshifted ion branch with $\omega - k\beta_b c \approx -\omega_{b+}$. Defining $\delta\omega = \omega - \omega_{e+}$ and $\delta k = k - k_0$, and paralleling the similar derivation of Eqs. (56) and (57), the dispersion relation in Eq. (52) for the positive-frequency electron branch with $\omega \approx +\omega_{e+}$ can be approximated by the quadratic form

$$\delta\omega(\delta\omega - \beta_b c \delta k) = -\Gamma_3^2 = -f \frac{\eta}{4} \frac{\omega_{pb}^4}{\omega_{e+}\omega_{b-}} \frac{(\omega_{b-}^2 + 2\nu_b^2)(\omega_{e+}^2 + 2\nu_e^2)}{(\omega_{b+}^2 - \omega_{b-}^2)(\omega_{e+}^2 - \omega_{e-}^2)}, \tag{58}$$

in the vicinity of the axial wavenumber $k_0\beta_b c = \omega_{e+} - \omega_{b-}$, and by

$$\delta\omega(\delta\omega - \beta_b c \delta k) = -\Gamma_4^2 = -f \frac{\eta}{4} \frac{\omega_{pb}^4}{\omega_{e+}\omega_{b+}} \frac{(\omega_{b+}^2 + 2\nu_b^2)(\omega_{e+}^2 + 2\nu_e^2)}{(\omega_{b+}^2 - \omega_{b-}^2)(\omega_{e+}^2 - \omega_{e-}^2)}, \tag{59}$$

in the vicinity of the axial wavenumber $k_0\beta_b c = \omega_{e+} + \omega_{b+}$.

We note from Eq. (52) that the negative-frequency electron branch in Eq. (52) with $\omega \approx -\omega_{e\pm}$ can also couple unstably with the various ion branches at appropriate axial wavenumbers with negative values. However, due to the symmetry properties of Eq. (52), the approximate dispersion relations are similar to the quadratic forms in Eqs. (56)–(59). The detailed stability properties of the axisymmetric hollowing mode at moderate beam intensities can be investigated by making use of Eqs. (56)–(59). The strength of the unstable coupling factors on the right-hand sides of Eqs. (56)–(59) for the hollowing mode is of the same order of magnitude as that in Eq. (36) for the sausage mode. Therefore, the maximum growth rates ($\Gamma_1, \Gamma_2, \Gamma_3$, and Γ_4) of the hollowing-mode instability are the same order-of-magnitude as the growth rate of the sausage instability.

For high intensity beams with $s_b = \omega_{pb}^2/2\gamma_b^2\omega_{\beta b}^2$ approaching unity, it is necessary to solve the full dispersion relation in Eq. (52) for the complex oscillation frequency ω . Typical numerical results obtained from Eq. (52) are illustrated in Fig. 4, where the normalized growth rate $u_i = (\text{Im}\omega)/\omega_{\beta b}$ is plotted versus the shifted axial wavenumber (a) $\zeta_- = (k\beta_b c - \omega_{e-})/\omega_{\beta b}$ and (b) $\zeta_+ = (k\beta_b c - \omega_{e+})/\omega_{\beta b}$ for the two classes of unstable modes described earlier in this section. In Fig. 4, the normalized beam intensity is $s_b = \omega_{pb}^2/2\gamma_b^2\omega_{\beta b}^2 = 0.5$, the fractional charge neutralization is $f = n_e/Z_b n_b = 0.1$, and system parameters are otherwise identical to Fig. 1. Moreover, the electron collective oscillation frequencies $\omega_{e\pm}$ are defined in Eq. (51). We remind the reader that the collective oscillation frequencies $\omega_{e\pm}$ of electrons are several orders in magnitude larger than the oscillation frequencies $\omega_{b\pm}$ in Eq. (50) of the beam ions due to the large mass ratio $\eta = \gamma_b m_b/Z_b m_e$. In this context, the axial wavenumbers k_0 defined in Eqs. (56) and (57) are given approximately by $k_0\beta_b c \approx \omega_{e-}$. Similarly, the axial wavenumbers k_0 defined in Eqs. (58) and (59) are given approxi-

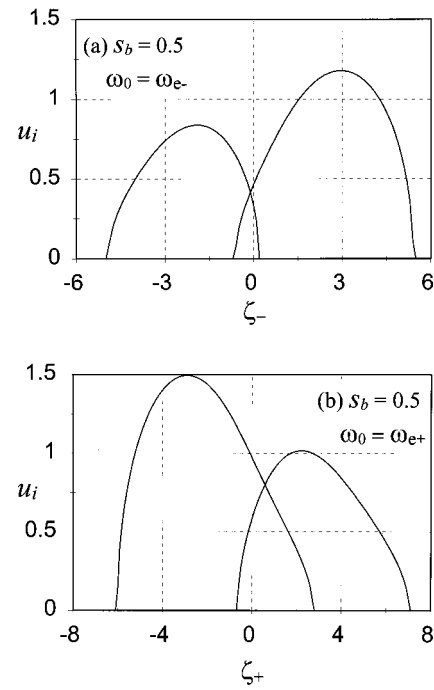


FIG. 4. Plots of the normalized growth rate $u_i = (\text{Im}\omega)/\omega_{\beta b}$ versus the shifted axial wavenumber (a) $\zeta_- = (k\beta_b c - \omega_{e-})/\omega_{\beta b}$ and (b) $\zeta_+ = (k\beta_b c - \omega_{e+})/\omega_{\beta b}$ obtained from Eq. (52) for normalized beam intensity $s_b = \omega_{pb}^2/2\gamma_b^2\omega_{\beta b}^2 = 0.5$, and parameters otherwise identical to Fig. 1.

mately by $k_0\beta_b c \approx \omega_{e+}$. Therefore, the left-most growth-rate curve in Fig. 4(a) obtained numerically from Eq. (52) corresponds to the approximate dispersion relation in Eq. (56), and the right-most growth-rate curve in Fig. 4(a) corresponds to Eq. (57). Similarly, the left-most growth-rate curve in Fig. 4(b) corresponds to Eq. (58), and the right-most growth-rate curve in Fig. 4(b) corresponds to Eq. (59).

We remind the reader that the axial wavenumbers corresponding to instability in Fig. 4(b) are far larger than those in Fig. 4(a). Although the growth-rate curves obtained from the approximate dispersion relations in Eqs. (56)–(59) are symmetric about the appropriately defined axial wavenumber $k = k_0$, each growth-rate curve in Fig. 4 obtained numerically from the full dispersion relation in Eq. (52) is skewed about $k = k_0$. In particular, the growth-rate curves in Fig. 4(a) are skewed to the left, whereas those in Fig. 4(b) are skewed to the right. Of course the growth-rate curves corresponding to one of the approximate dispersion relations in Eqs. (56)–(59) are valid at lower values of beam intensity, and are symmetric about the appropriate values of k_0 .

In conclusion, we note from Figs. 1 and 4 that the growth rate of the hollowing instability ($n=2$) is comparable to that of the sausage instability ($n=1$). In this context, we conclude that the axisymmetric hollowing instability may also be deleterious to intense ion beam propagation through a background population of electrons.

V. CONCLUSIONS

In this paper, we have investigated two-stream stability properties for axisymmetric perturbations in an intense ion beam propagating through background electrons, by making

use of the Vlasov–Maxwell equations. The basic assumptions and theoretical model were presented in Sec. II. The theoretical model is based on the linearized Vlasov–Maxwell equations for perturbations with long axial wavelength ($k^2 r_b^2 \ll 1$). The eigenfunctions for axisymmetric radial modes were introduced, and the dispersion relation was determined self-consistently by evaluating the orbit integral for the perturbed distribution function in closed analytical form.

Stability properties of the sausage mode, characterized by the radial mode number $n=1$ were investigated in Sec. III. The dispersion relation for the sausage mode was expressed in a quadratic form, similar to the dispersion relation for the hose instability (dipole-mode).¹⁶ The eigenfunction obtained self-consistently for the sausage mode indicates that the perturbations exist only inside the beam. Therefore, the presence of the grounded conducting wall does not affect the stability behavior. Stability properties of the hollowing instability, characterized by radial mode number $n=2$, were investigated in Sec. IV. The full dispersion relation for the hollowing mode was obtained, which predicts instability in several ranges of axial wavenumber k . The growth rates of the sausage and hollowing instabilities are of the same orders of magnitude as that of the dipole-mode hose instability.¹⁶ In this regard, we emphasize that the axisymmetric sausage and hollowing instabilities may also be deleterious to intense ion beam propagation through background electrons.

ACKNOWLEDGMENTS

This research was supported by the U.S. Department of Energy, and in part by the Spallation Neutron Source Project.

¹R. C. Davidson, *Physics of Nonneutral Plasmas* (Addison-Wesley, Reading, MA, 1990), and references therein.

²A. W. Chao, *Physics of Collective Beam Instabilities in High Energy Accelerators* (Wiley, New York, 1993).

³M. Reiser, *Theory and Design of Charged Particle Beams* (Wiley, New York, 1994).

⁴J. D. Lawson, *The Physics of Charged-Particle Beams* (Oxford Science, New York, 1988).

⁵R. A. Jameson, in *Advanced Accelerator Concepts*, American Institute of Physics Conference Proceedings 279, edited by J. S. Wurtele (American Institute of Physics, New York, 1993), p. 969.

⁶E. P. Lee and J. Hovingh, *Fusion Technol.* **15**, 369 (1989).

⁷*Proceedings of the 1995 International Symposium on Heavy Ion Inertial Fusion*, edited by J. J. Barnard, T. J. Fessenden, and E. P. Lee; *J. Fusion Eng. Design* **32**, 1 (1996), and references therein.

⁸D. G. Koshkarev and P. R. Zenkevich, *Part. Accel.* **3**, 1 (1972).

⁹R. C. Davidson and H. S. Uhm, *J. Appl. Phys.* **51**, 885 (1980).

¹⁰R. C. Davidson and H. S. Uhm, *Phys. Fluids* **21**, 60 (1978).

¹¹D. Neuffer, E. Colton, D. Fitzgerald, T. Hardek, R. Hutson, R. Macek, M. Plum, H. Thiessen, and T. S. Wang, *Nucl. Instrum. Methods Phys. Res. A* **321**, 1 (1992).

¹²D. Neuffer and C. Ohmori, *Nucl. Instrum. Methods Phys. Res. A* **343**, 390 (1994).

¹³M. Izawa, Y. Sato, and T. Toyomasu, *Phys. Rev. Lett.* **74**, 5044 (1995).

¹⁴J. Byrd, A. Chao, S. Heifets, M. Minty, T. O. Roubenheimer, J. Seeman, G. Stupakov, J. Thomson, and F. Zimmerman, *Phys. Rev. Lett.* **79**, 79 (1997).

¹⁵E. Keil and B. Zotter, CERN Report No. CERN_ISR-TH/71-58 (CERN Scientific Information Services, Geneva, 1971).

¹⁶R. C. Davidson, P. H. Stoltz, and T. S. Wang, *Phys. Rev. ST Accel. Beams* **2**, 054401 (1999).

¹⁷R. C. Davidson and H. S. Uhm, *Phys. Lett. A* **285**, 88 (2001).

¹⁸E. P. Lee, *Phys. Fluids* **21**, 1327 (1978).

¹⁹H. S. Uhm and M. Lampe, *Phys. Fluids* **23**, 1574 (1980).

²⁰H. S. Uhm and M. Lampe, *Phys. Fluids* **24**, 1553 (1981).

²¹G. Joyce and M. Lampe, *Phys. Fluids* **26**, 3377 (1983).

²²H. S. Uhm and R. C. Davidson, *Phys. Fluids* **23**, 1586 (1980).

²³R. L. Gluckstern, in *Proceedings of the 1970 Proton Linac Conference*, edited by M. R. Tracy (National Accelerator Laboratory, Batavia, IL, 1970), p. 811.

²⁴T.-S. Wang and L. Smith, *Part. Accel.* **12**, 247 (1982).

²⁵I. M. Kapchinskij and V. V. Vladimirskij, in *Proceedings of the International Conference on High Energy Accelerators and Instrumentation* (CERN Scientific Information Services, Geneva, 1956), Vol. I, p. 68.

²⁶W. W. Lee, Q. Qian, and R. C. Davidson, *Phys. Lett. A* **230**, 347 (1997).

²⁷I. Hofmann, L. Laslett, L. Smith, and I. Haber, *Part. Accel.* **13**, 145 (1983).

²⁸I. Haber and A. W. Maschke, *Phys. Rev. Lett.* **42**, 1479 (1979).